Supplemental Information

ABRUPT AND GRADUAL EXTINCTION AMONG LATE PERMIAN LAND VERTEBRATES IN THE KAROO BASIN, SOUTH AFRICA

Peter D. Ward,* Jennifer Botha, Roger Buick, Michiel O. De Kock, Douglas H. Erwin, Geoffrey Garrison, Joseph Kirschvink, and Roger Smith

* To whom correspondence should be addressed . E-mail: argo@u.washington.edu

Paleomagnetic Measurement Methods

One previous paleomagnetic study of these sediments in the western portion of the Cape fold belt of Southern Africa revealed a pervasive remagnetization associated with Mesozoic deformation and the intrusion of dolerite dikes and sills (*1*); sediments along the margin of the Cape fold belt acquired their NRM after deformation of the strata, presumably as a result of thermochemical alteration. For our paleomagnetic studies we report results from three paleontologically well-constrained sections in the flat-lying Karoo well away from this fold belt which span the Permian/Triassic boundary. Two of these are in the vicinity of Lootsberg Pass (*2*), along each stretch of the highway, East and West of the summit, merging at the top. We also intensively sampled a 5m thick sequence of the Permian/Triassic 'Event beds" at Carlton Heights (*3*). In addition, results from a smaller section at Komandodriftam have been reported recently (*4*).

Paleomagnetic samples were obtained using standard techniques with gasoline powered drills and 2.5 cm diameter diamond coring bits. Cores were oriented *in situ* with a magnetic compass and, where possible, by sun compass. All samples were analyzed at

the California Institute of Technology paleomagnetics laboratory, using a 3-axis DC-SQUID moment magnetometer system housed in a magnetically shielded μ-metal room. The background noise of this instrument is less than 1 picoA·m^2, and it is equipped with a vacuum pick-and-put, computer-controlled sample handling system which can measure up to 180 samples automatically (*5*). AF demagnetization was performed with a computer-controlled, three-axis coil system. Thermal demagnetization was performed in a commercially-built magnetically shielded furnace.

All samples were initially measured for natural remnant magnetization, and then subjected to low AF demagnetization up to 10 mT at ~2 mT steps to remove low coercivity magnetizations. The samples were then treated with thermal demagnetization from 100°C in ~25° C increments to 525° C, in 15 or 20° C increments to 640° C, and when warranted, several more steps up to 688° C or until they became unstable (Fig. S1). Approximately 4,800 demagnetization experiments and associated magnetic measurements were performed on the 184 samples, or about 26 demagnetization steps per sample. In all but the low-field Af demagnetization steps, we used 8 sets of complete vector measurements (4 up-arrow, 4 down arrow) to assess the stability.

Three general rock types were analyzed in this study, blue-green claystone and sandstone, reddish claystone and sandstone, and the medium-grained dolerite dikes that intrude throughout the Karoo (*6*). The majority of samples could be characterized as well-behaved, with most possessing a component of low Af and thermal stability similar to the present magnetic field direction in Southern Africa, as well as one or two additional components of higher thermal stability. Demagnetization data were analyzed using principal component analysis to isolate stable magnetic directions (*7*) and to assess the

polarity of samples with multiple components. Only demagnetization lines with MAD values below 10°, and planes below 15°, were included in the statistical analysis. Mean directions were obtained using Fisher statistics (*8*), and the method of McFadden & McElhinny (*9*) was used for combining data from demagnetization lines and arcs, and the final iterative directions along the arc constraints were combined with lines for the stratigraphic polarity interpretation. The reversals test followed that of McFadden & McElhinny (*10*). Cleaned directional data from the sampling sites (Fig. S2) show a baked contact test near the base of the West Lootsberg Pass section.

Dolerite dikes of the Karoo intrusive complex (*6*) are present in the Lootsberg pass area, but appear absent at the Carlton Heights locality. West Lootsberg Pass has a single vertical dike ~4 m thick, which crosses the section three times, once at the ~ 15 m level in the stream cut near the bottom of the section, again in the road cut near the ~160 meter level, and once again at the summit of the combined East and West Lootsberg Pass sections (Fig. S3). Fossil bone samples collected away from this intrusion are light in color, but within ~10m of the dike they darken progressively. Demagnetization experiments on samples of the dolerite isolate a consistent Southeast and shallow magnetic direction, nearly 40 degrees away from that of either the expected Permo-Triassic reversed field for southern Gondwana (*11*) or the mean direction in the Karoo intrusive suite (*6*). This is fortuitous, as this angular separation is enough to permit reliable identification of the dolerite-induced remagnetization direction in the Lootsberg Pass samples. This also implies that the time scale for the emplacement of the intrusion in this area was short relative to the time scale of secular variation, as all units in the Pass area yield essentially the same direction. Figure S1 shows examples of the

demagnetization behavior of three of the red siltstone samples which have been partially or totally remagnetized by this intrusion near the base of the West Lootsberg Pass section. At low demagnetization steps a present field component is removed, and the magnetic vectors follow great circle arcs headed towards the dolerite direction on the equal-area projections. At higher temperatures, however, magnetic vectors in the two samples furthest from the intrusion change their trajectory and move on similar great-circle arcs towards the Permo/Triassic normal polarity direction. The demagnetization temperature at which this happens decreases with distance from the intrusion, as is expected from a thermomagnetic overprint. The sample closest to the sill has been remagnetized entirely. This constitutes a positive baked contact test for the high-temperature component (*12*), indicating that it predates intrusion of the dolerite. Unfortunately, most of the greenish samples are located in the stream exposures in the lower part of the section, and appear to have been remagnetized by the intrusion. Note that at Komandodriftam, both the greenish and reddish sediments are capable of preserving primary directions, if free from surface weathering (*4*).

Careful thermal demagnetization experiments on the reddish samples in the temperature range from 550 to 688°C usually yields clear great-circle arcs towards either the Permo/Triassic normal or reversed directions, which commonly end in a stable direction. The two groups of directions pass the reversals test with a "B" classification (*10*) as indicated in Table S1.

The major problem in the paleomagnetic studies described here and by De Kock & Kirschvink (*4*) is the ability to distinguish the Karoo Permian-Triassic Normal direction from that of the Present Local Field, (PLF), which are separated by an angular

distance of only 15º, implying that the scatter cones of their Fisherian distributions overlap. At first, this problem appears somewhat intractable, as the sediments are essentially flat-lying and the present field overprint is pervasive. However, at the Lootsberg pass locality it became clear during examination of the Normally magnetized interval approaching the basal dolerite sill mentioned above that the weathering effects were, in general, removed at the lower Af and thermal demagnetization steps (≤ 400° C). This PLF component had essentially intruded upon the portion of the stability spectrum that had been remagnetized by the intrusion. Above these temperatures it was usually possible to observe motion of the NRM vector towards a high-temperature, Permian/Triassic Boundary (PTB) Normal direction (Fig. S2). These components could either be isolated by principal component analysis on the high-temperature steps, or via the use of great-circle arc constraints as noted above. Examination of the samples higher up in this sequence reveal that the same technique also works on those samples interpreted to be in the Reversed polarity interval, with small arcs moving away from the Present direction towards the SE and down PTB Reversed direction. Figure S2 shows the arc constraints on these directions. This approach tends to be conservative for the Normal polarity directions, as those samples that contain a primary component too similar to that of the present field direction (no directional change in position with demagnetization) are simply not used in the analysis. Although this occasional exclusion does bias the mean group of Normal directions slightly away from the true mean, and is the probable cause of the slight deviation from antiparallelism in the Normal and Reversed polarity groups shown on Table S1, the polarity interpretation is conservative.

A clear stratigraphic distinction exists in these sections, and all samples below the 130 m mark at Lootsberg West display normal polarity and those above show only reversed polarity (Fig. S3), with the exception of a small group of samples above the point where these two sections merge. In conjunction with the reversal (R/N) found by De Kock & Kirschvink (*4*) at the Komandodriftdam locality, which is slightly below the P/T boundary event beds (*13*), this yields a pattern of four magnetic polarity Chrons, which we are designating R1/N1/R2/N2. The P/T boundary, as determined from vertebrate paleontology, lies above the base of Chron N1. We interpret our Chron N1 to be correlative to the basal Triassic Normal Chron identified in many other parts of the world, in both marine and terrestrial sediments (*14, 15*), but we note with some dismay that this marine extinction horizon has been suggested to be either near the base of this Normal Chron, as it is here, or in the uppermost portion of the underlying Reversed Chron (see (*16*) for a discussion).

The combination of the baked contact test, the reversals test, and the presence of layer-bound magnetic polarity zones strongly implies that the magnetization was acquired at or shortly after the time of deposition. Given the robust number of samples yielding useable results, and the excellent age constraints on the Permian/Triassic boundary (*17, 18*), the mean direction rates a perfect 7 on the 7-point paleomagnetic quality (Q) index of Van der Voo (*19*), and indicates a paleolatitude of ~ 41° S.

Table S1. Summary of paleomagnetic Fisherian statistics from the Lootsberg Pass and Carlton Heights sections. No structural correction has been made because the sediments are flat-lying. Data for the dolerite overprint direction include samples from the dike as well as remagnetized sediments. 'N_{eff}' indicates the effective number of samples in the

analysis, and (L, P) give the number of individual demagnetization Lines and Planes, respectively (N_{eff} = L + ½P; see (*9*)) . As separate groups, the Normal and Reversed directions pass the paleomagnetic reversals test with "B" classification (*10*). The summit of Lootsberg Pass, South Africa, is located at 31° 50.133' S, 24° 51.607' E, and Carlton Heights is at 31° 19.898' S, 24° 58.521' E. Raw demagnetization data, least-squares tables, and sample-by-sample interpretations will be posted at http://www.gps.caltech.edu/MagLab/ before publication.

East & West Lootsberg Pass, and Carlton Heights

	N(eff.)	(L, P)	Decl.	Incl.	α95	κ
PLF, overprint	93.0	(93, 0)	335.8	-59.3	1.7	76.46
OVP, dolerite overprint	37.5	(33, 9)	117.4	13.6	3.7	41.23
NOR, primary	45.5	(41,9)	303.3	-61.0	4.0	28.36
REV, primary	25.5	(5, 41)	133.1	57.1	4.3	46.27
NOR+REV	71.0	(46, 50)	307.1	-59.8	3.0	32.53

The pole is at 47.1 N, 267.6 E, (dp, dm) = (2.4, 4.5), paleolatitude -40.7 (-34.7/-44.2)

Komandodrift-dam (De Kock & Kirschvink, 2004)

	N(eff.)	(L, P)	Decl.	Incl.	α95	κ
NOR + REV	21.0	(7, 28)	311.9	-61.6	7.6	17.80

The mean directions from these studies are not statistically distinguishable (Gr = 0.8, Chi^2 p. value 0.668)

Supplemental Paleomagnetics References:

1. V. Bachtadse, R. Vandervoo, I. W. Halbich, *Earth and Planetary Science Letters* **84**, 487 (1987).
2. G. H. Groenewald, J. W. Kitching, in *Biostratigraphy of the Beaufort Group (Karoo Supergroup)* B. S. Rubidge, Ed. (Council for Geosciences, South African Committee for Stratigraphy, Geological Society of South Africa, 1995), vol. 1, pp. 35-39.
3. M. B. Steiner, Y. Eshet, M. R. Rampino, D. M. Schwindt, *Palaeogeography Palaeoclimatology Palaeoecology* **194**, 405 (May 25, 2003).
4. M. O. De Kock, J. L. Kirschvink, *Gondwana Research* **7**, 175 (2004).
5. J. L. Kirschvink, paper presented at the Spring AGU Meeting, Boston, MA 2002.

6. R. B. Hargraves, J. Rehacek, P. R. Hooper, *South African Journal of Geology* **100**, 195 (1997).
7. J. L. Kirschvink, *Geoph. J. Royal Astr. Soc.* **62**, 699 (1980).
8. R. A. Fisher, *Porc. R. Soc. A* **217**, 295 (1953).
9. P. L. Mcfadden, M. W. McElhinny, *Earth & Planetary Science Letters* **87**, 161 (1988).
10. P. L. McFadden, M. W. McElhinny, *Geophysical Journal Int.* **103**, 725 (1990).
11. F. Torq, e. al., *Earth and Planetary Science Letters* **148**, 553 (1997).
12. R. F. Butler, *Paleomagnetism : magnetic domains to geologic terranes* (Blackwell Scientific Publications, Boston, 1992), pp. 319.
13. R. M. H. Smith, P. D. Ward, *Geology* **29**, 1147 (Dec, 2001).
14. M. Szurlies, G. H. Bachmann, M. Menning, N. R. Nowaczyk, K. C. Kading, *Earth and Planetary Science Letters* **212**, 263 (Jul 25, 2003).
15. M. Steiner, J. Ogg, Z. Zhang, S. Sun, *J. Geophysical Research* **94**, 7343 (1989).
16. J. Nawrocki, *Terra Nova* **16**, 139 (Jun, 2004).
17. S. A. Bowring *et al.*, *Science* **280**, 1039 (May 15, 1998).
18. P. R. Renne, Z. C. Zhang, M. A. Richards, M. T. Black, A. R. Basu, *Science* **269**, 1413 (Sep 8, 1995).
19. R. Van der Voo, *Palaeomagnetism of the Atlantic, Tethys, and Iapetus Oceans* (Cambridge University Press, Cambridge, U.K., 1993), pp. 411.
20. P. D. Ward, D. R. Montgomery, R. Smith, *Science* **289**, 1740 (Sep 8, 2000).

Figure S1. Demagnetization data for the baked contact test. Samples BGLP- 179, 180, and 181 are red siltstones collected from near the base of the West Lootsberg Pass section where it approaches the vicinity of the dolerite dike, as indicated on Fig. S3. On the equal area diagrams here the solid (open) symbols indicate downwards (upwards) magnetic directions. On the orthogonal projections, the red symbols indicate projection of the remanence vector into the horizontal plane, and blue symbols are the corresponding projection into the East/West vertical plane. The high-temperature component becomes progressively weaker, and the dolerite overprint component stronger, as the sampling locality approaches the dike.

Figure S2. Equal-area plots showing the principal magnetic components isolated from the demagnetization data generated in this study. Directions obtained from linear components are shown as squares, and the arc-segments show the constraints from demagnetization planes (*9*). Overprint directions shown on the left-hand diagram include those attributed to chemical and viscous remagnetization during weathering in the present geomagnetic field, and that of the mid-Mesozoic field which was present during the intrusion and cooling of the dolerite sill. The right-hand diagram shows the high-temperature, two polarity component interpreted as the primary Permo-Triassic field direction. Although the mean Normal polarity P/T direction is similar to that of the present field overprint, they are separated easily by the large difference in their thermal stability properties as shown on Fig. S1. Statistical data for these components are given in Table S1.

Figure S3. Range data for Permian and lower Triassic strata in Karoo basin, compiled from ref 16 and the new data presented here. Each taxon is a genus. This graph supports

our contention that significant background extinction was occurring well before the P/T event. While no equivalent graph plotted such as that presented here exists for the Hell Creek formation (with a time span of about half that shown in the Permian part of this diagram), the work of (*9*) has demonstrated that at least among dinosaurs there no decrease in taxa prior to the K/P event occurred.

Supplemental Materials: Stable Isotopic Measurement Methods

Inorganic carbonate $\delta^{13}C$ ($\delta^{13}C_{carb}$) data comes from paleosol carbonate nodules, while the bulk sedimentary organic carbon isotope record ($\delta^{13}C_{org}$) comes from fine-grained pond and overbank deposits. Carbonate soil nodule ^{13}C:^{12}C ratios are controlled by temperature and pore space $\delta^{13}C_{CO2}$. Pore space $\delta^{13}C_{CO2}$ is controlled by both the CO_2 produced *in situ* from the microbial remineralization of buried organic matter (i.e., respired CO_2), and atmospheric CO_2 diffusing into the soil. Thus, the nodule $\delta^{13}C_{carb}$ ratio is affected not only by the $\delta^{13}C_{CO2}$ but also the partial pressure of CO_2 (pCO_2) in the atmosphere; a negative excursion in soil nodule $\delta^{13}C_{carb}$ can be caused by both a decrease in $\delta^{13}C_{CO2}$ and an increase in atmospheric pCO_2. Sedimentary organic ^{13}C:^{12}C ($\delta^{13}C_{org}$) was analyzed via elemental analyzer–continuous-flow isotope ratio mass spectrometry (EACFIRMS) at the Stable Isotope Research Facility (SIRF); SIRF is operated jointly by the Quaternary Research Center and the Astrobiology Program at the University of Washington. Powdered samples were first acidified with >5 ml 10% HCl per mg of sample material and kept at 40°C for at least 12 hr to remove inorganic carbonate material. Samples were then triple rinsed with ultrapure (>18 MΩ) deionized

water and oven dried at 40°C. Total carbonate removal by this procedure was verified by measuring $\delta^{13}C_{org}$ during a series of repeated acid leaching tests on six samples from the Lootsberg section (Fig. S5). Analyses were made with a Costech ECS 4010 Elemental Analyzer coupled to a ThermoFinnigan MAT253 mass spectrometer via a ThermoFinnigan CONFLO III gas interface. Carbonate mineral ^{13}C:^{12}C ($\delta^{13}C_{carb}$) and ^{18}O:^{16}O ($\delta^{18}O_{carb}$) were measured by IRMS on a Micromass Isoprime dual inlet mass spectrometer. Samples were introduced via a Micromass carbonate autosampler system. Samples were held in evacuated 5 ml vacutainers with proprietary CO_2-impermeable seals and acidified with 103% phosphoric acid at 90°C for 10 minutes; the evolved CO_2 was cryogenically stripped of water vapor prior to being introduced to the mass spectrometer. Isotope ratios are reported in standard delta (δ) notation relative to Vienna Pee Dee Beleminite (VPDB), where $\delta^{13}C = [[(^{13}C/^{12}C)\ sample/(^{13}C\ /^{12}C)\ VPDB]-1]*1000$; internal laboratory reference materials for $\delta^{13}C$ and $\delta^{18}O$ analyses have been calibrated against NBS-19 (calcite; $\delta^{13}C$ = +1.95‰, $\delta^{18}O$ = -2.20‰, VPDB). The standard deviation (σ) of sample replicates was 0.15‰ for $\delta^{13}C_{org}$ (n = 36), 0.10‰ for $\delta^{13}C_{carb}$ (n = 50), and 0.25‰ for $\delta^{18}O_{carb}$ (n = 50). Analytical precision based on routine analyses of internal laboratory reference materials was 0.15‰ for $\delta^{13}C_{org}$ and 0.21‰ for $\delta^{13}C_{carb}$ and $\delta^{18}O_{carb}$.

Results from tests of our carbonate removal techniques. (a) $\delta^{13}C_{org}$ vs. increasing ml 10% HCl:mg sample ratio of six samples taken from the Lootsberg section. Three mg of 10% HCl per mg of sample was considered the minimum acid:sample ratio to remove carbonate material from the samples. (b) $\delta^{13}C_{org}$ vs. heating duration of the same samples in (a) having been treated with 4 ml 10% HCl per ug of sample material. Twenty-four hours was considered enough time at 40°C to remove any recalcitrant carbonate mineral phases such as siderite and dolomite.

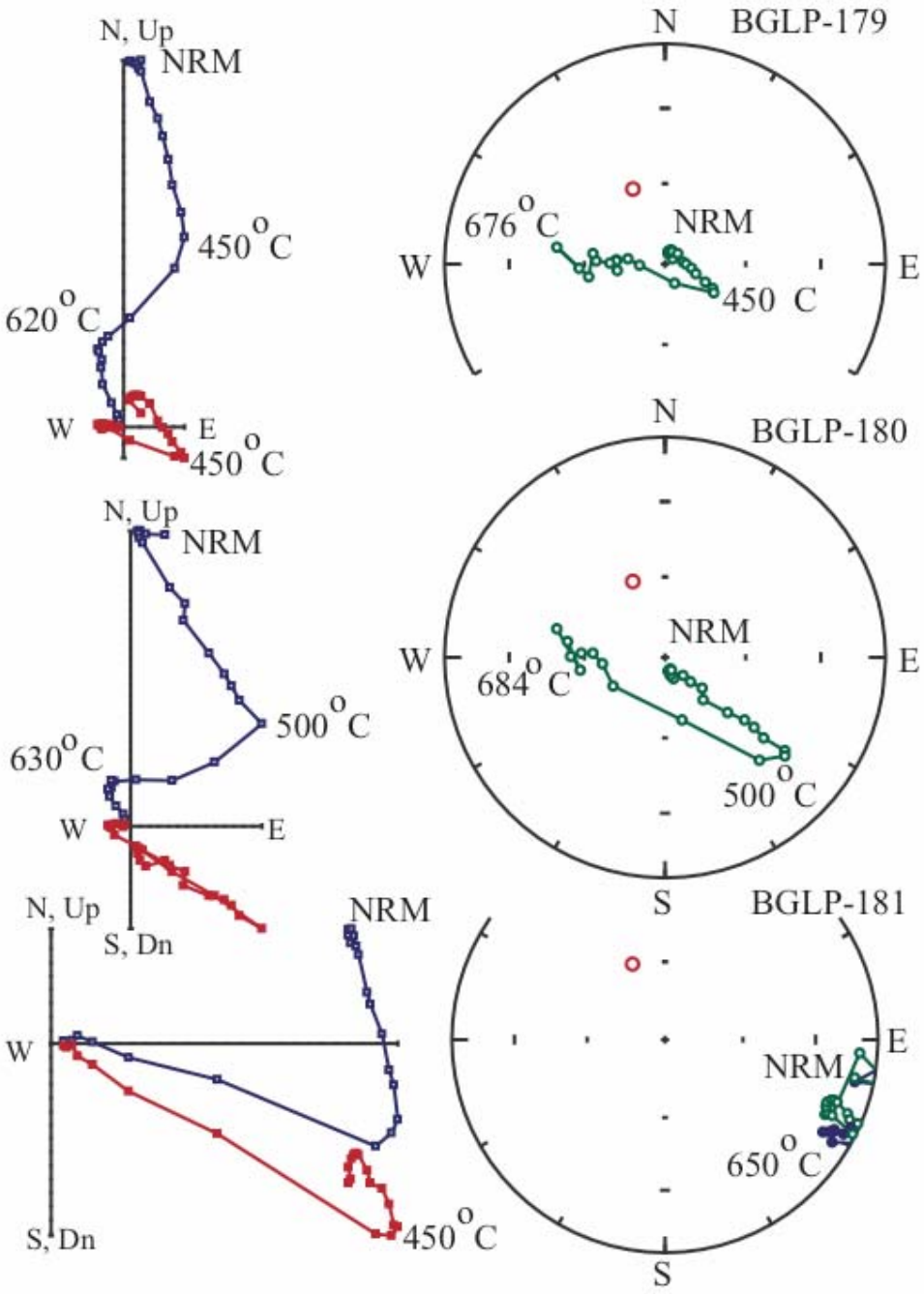

Fig. S1, Ward et al.

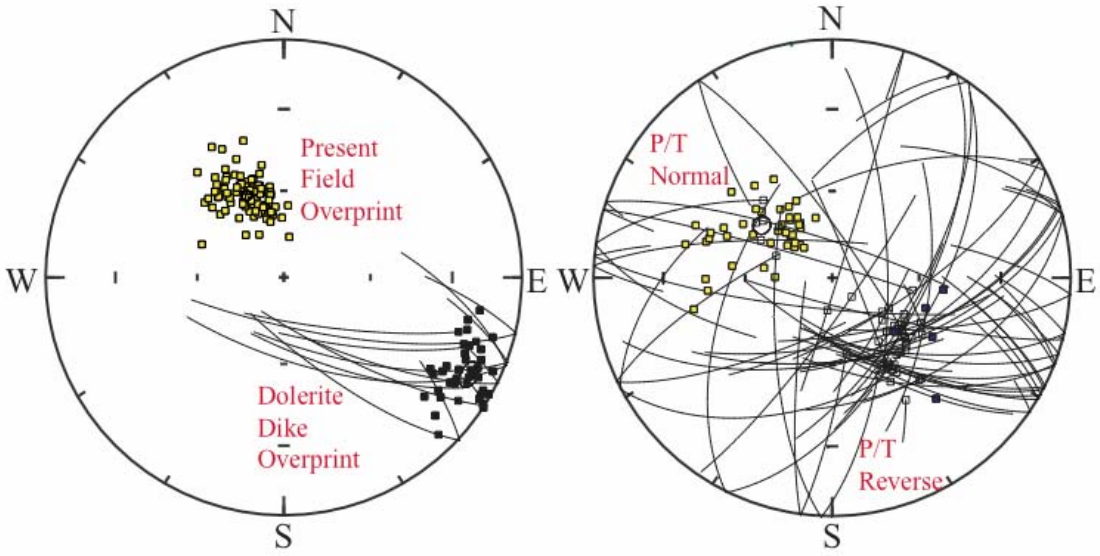

Fig. S2 Ward et al.

a. **b.**

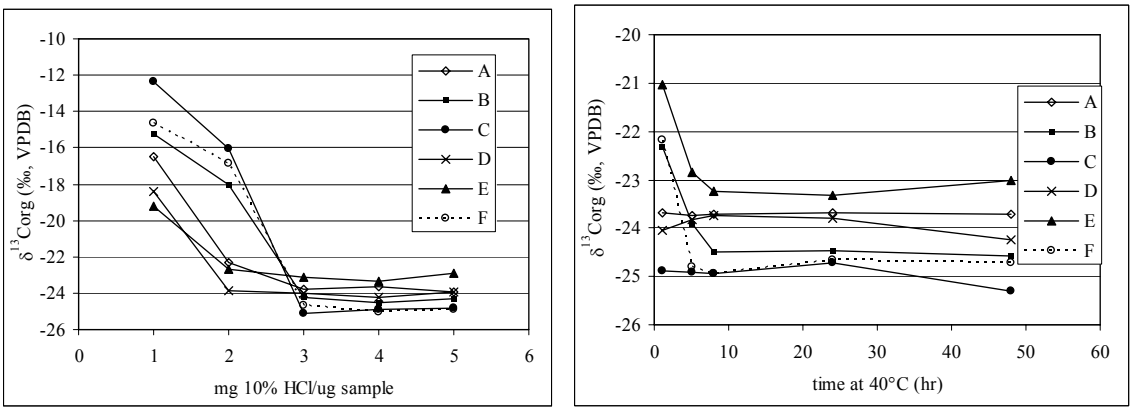

Figure S3 Ward et al.

Table S2. Sedimentary stable carbon isotope data

WAPATS BERG						BETHULIE					CARLTON HEIGHTS					LOOTSBERG				
ID1	ID2	Strat. position (m)	No. of analyses	δ^{13}Corg (‰, VPDB)	SD	ID	Strat. position (m)	No. of analyses	δ^{13}Corg (‰, VPDB)	SD	ID	Strat. position (m)	No. of analyses	δ^{13}Corg (‰, VPDB)	SD	ID	Strat. position (m)	No. of analyses	δ^{13}Corg (‰, VPDB)	SD
11/21/01	47	25.5	1	-24.04		26	19.6	2	-24.18	1.13	61	36.9	1	-22.89		49	34.6	4	-23.63	0.03
11/21/01	46	22.2	1	-24.54		25	19.45	2	-23.85	0.29	60	35.1	3	-22.73	0.24	47	33.3	3	-22.19	0.17
11/21/01	45	19.9	1	-24.31		24	18.8	2	-23.30	0.11	59	34.45	2	-23.36	0.00	46	32.9	2	-21.63	0.36
11/21/01	44	18.75	1	-24.19		23	18.05	2	-23.66	0.22	58	33.5	3	-23.26	0.34	45	32.2	4	-21.85	0.52
11/21/01	43	17.85	2	-24.29	0.11	22	17.3	2	-23.80	0.14	57	32.5	2	-23.51		44	31.2	2	-21.82	0.60
11/21/01	42	16.2	2	-24.95	0.44	21	16.7	2	-23.29	0.10	56	31.7	2	-23.63	0.53	43	30.15	2	-22.61	0.11
11/21/01	41	15	1	-24.35		20	15.3	2	-23.40	0.01	55	30.9	3	-22.65	0.24	42	29.5	2	-22.38	0.00
11/21/01	40	14	2	-24.26	0.28	19	14.2	2	-23.31	0.06	54	28	3	-22.67	0.04	41	28.7	4	-23.42	0.06
11/21/01	39	13.05	2	-23.33	0.61	18	13.3	2	-23.31	0.10	53	27	2	-22.88	0.00	40	27.65	4	-22.02	1.06
11/21/01	38	12.5	1	-23.41		17	12.1	2	-22.76	0.11	52	26.15	2	-22.53	0.00	39	27.15	3	-22.08	0.25
11/21/01	37	11.95	1	-24.12		16	11.1	2	-23.16	0.52	51	25.3	1	-23.36		38	26.9	2	-22.59	0.08
11/21/01	36	11.25	1	-23.83		15	10.2	2	-23.30	0.06	50	24.35	3	-22.77	0.19	37	22.35	4	-21.95	0.38
11/21/01	35	10.85	1	-23.38		14	8.6	2	-23.34	0.31	49	24.05	3	-22.64	0.11	36	22.2	2	-21.96	0.90
11/21/01	33	10.3	1	-23.13		13	8.1	1	-24.03		48	23.1	3	-22.61	0.03	35	21.35	3	-21.55	0.58
11/21/01	32	10.1	1	-23.43		12	7.35	2	-23.10	0.34	47	22.8	3	-22.81	0.24	34	20.05	4	-22.54	0.45
11/21/01	31	9.9	1	-23.32		11	6.8	2	-24.73	0.29	46	21.4	3	-23.01	0.07	33	20.00	4	-23.17	1.11
11/21/01	29	9.45	1	-22.87		10	4.15	2	-24.28	0.47	44	20	2	-22.98		32	18.45	2	-24.74	0.01
11/21/01	28	9.15	1	-23.70		9	3.5	3	-22.95	0.39	43	19.9	3	-22.55	0.15	31	17.7	2	-24.28	0.09
11/21/01	27	8.45	3	-24.04	0.77	8	2.75	2	-22.79	0.03	42	19.1	2	-22.35		30	17.4	2	-24.80	0.06
11/21/01	26	7.9	1	-24.89		7	2.05	2	-23.57	0.05	3	18.8	2	-23.23	0.29	29	17	2	-24.94	0.08
11/21/01	25	7.1	3	-23.17		6	1.4	2	-23.85	0.10	4	18.7	3	-23.68	0.25	28	15.1	3	-24.34	0.00
11/21/01	24	6.4	3	-22.95	0.51	5	1.15	2	-24.11	0.83	5	18.55	2	-24.71	0.58	27	13.55	2	-25.10	0.16
11/21/01	23	5.9	3	-22.46	0.90	4	0.85	1	-24.55		9	17.85	4	-23.81	0.20	25	10.7	2	-25.38	0.45
11/21/01	22	5.45	4	-24.41	0.03	3	0.4	2	-23.69	0.13	10	17.6	2	-23.58	0.44	24	10	2	-24.56	0.36
11/21/01	21	5.05	2	-23.94	0.35	2	0	2	-23.75	0.06	11	17.15	2	-23.66	0.12	23	8.45	2	-24.67	0.28
11/21/01	20	4.75	2	-24.16	0.82	1	-0.01	3	-23.49	0.22	12	16.65	1	-23.51		22	8.25	1	-24.97	
11/21/01	16	4.55	2	-22.86		27	-0.35	2	-23.61	0.12	13	16.3	1	-23.97		21	7.8	6	-24.98	0.93
11/21/01	15	4.25	2	-22.75		28	-1.25	3	-24.07	0.51	14	15.95	2	-24.35	0.47	20	6.35	4	-24.48	0.66
11/21/01	14	3.9	2	-23.84	0.79	32	-1.65	2	-23.52	0.01	15	15.7	3	-24.10	0.23	19	6.05	4	-24.94	0.79
11/21/01	13	3.35	2	-23.77	0.56	29	-1.8	3	-23.45	0.59	16	14.9	2	-25.30	0.15	18	5.6	2	-24.39	0.34
11/21/01	12	3.15	2	-24.63	0.24	30	-2.65	2	-23.78	0.22	17	14.45	3	-24.46	0.39	17	4.7	3	-22.50	0.11
11/21/01	11	2.95	5	-24.30	0.63	31	-3.5	2	-24.13	0.03	18	14.15	1	-23.80		16	4.3	4	-23.63	0.76
11/21/01	10	2.6	4	-25.19	0.35	33	-6	2	-24.35	0.10	20	13.05	4	-24.13	0.12	14	3.3	4	-24.36	0.30
11/21/01	9	2.35	3	-24.64	0.47	34	-7.65	2	-22.77	0.25	21	11.95	2	-23.44	0.00	13	3	2	-25.02	0.21
11/21/01	8	2.1	4	-24.16		35	-9.4	2	-23.43	0.06	22	11	4	-25.42	0.19	12	2.75	3	-23.62	0.83
11/21/01	7	1.65	2	-23.79	0.29	36	-11.1	3	-23.57	0.23	23	10.35	4	-24.04	0.21	10	2.25	2	-24.69	0.46
11/21/01	6	1	4	-23.41	0.23	37	-12.4	4	-23.64	0.43	24	9.75	4	-25.32	0.31	9	2	1	-24.78	
11/21/01	5	0.8	1	-23.18		38	-13.8	2	-23.69	0.32	25	8.95	4	-24.52	0.30	8	1.75	2	-24.48	0.34

WAPATS BURG

ID#1	ID#2	Strat. position (m)	No. of analyses	δ^{13}Corg (‰, VPDB)	SD
11/21/01	1a	0.5	1	-22.74	
11/21/01	3	0.4	5	-23.00	0.34
11/21/01	2	0.15	4	-23.18	0.53
11/20/01	2	0	2	-25.76	0.59
11/21/01	17	-0.2	3	-22.90	0.55
11/21/01	18	-0.4	2	-23.34	0.55
11/20/01	3	-0.55	2	-25.51	0.55
11/21/01	19	-0.75	5	-23.71	1.20
11/20/01	4	-0.9	2	-24.96	0.18
11/20/01	5	-1.35	4	-23.40	0.34
11/20/01	6	-2.1	2	-24.28	0.08
11/20/01	7	-2.55	2	-23.97	0.09
11/20/01	8	-3.15	2	-23.38	0.23
11/20/01	9	-3.8	2	-23.75	0.08
11/20/01	10	-5.15	2	-24.02	0.05
11/20/01	12	-6.25	2	-25.46	0.16
11/20/01	13	-7	2	-23.96	0.38
11/20/01	14	-8	2	-23.73	0.01
11/20/01	15	-9.05	2	-24.33	0.26
11/20/01	16	-10.3	2	-23.35	0.15
11/20/01	17	-11.9	2	-24.22	0.40
11/20/01	18	-12.7	2	-23.63	0.11
11/20/01	19	-16.05	2	-24.27	0.67
11/20/01	20	-16.85	2	-23.83	0.14
11/20/01	21	-18.05	1	-23.17	

BETHULIE

ID	Strat. position (m)	No. of analyses	δ^{13}Corg (‰, VPDB)	SD
41	-17.2	2	-23.12	0.06
42	-18.8	2	-22.40	0.00
43	-20	2	-22.49	0.15

CARLTON HEIGHTS

ID	Strat. position (m)	No. of analyses	δ^{13}Corg (‰, VPDB)	SD
30	5.7	1	-25.08	
31	4.8	2	-24.29	0.45
32	4	1	-22.62	
33	2.75	3	-23.96	0.33
36	1.1	1	-24.66	
37	0.6	2	-23.90	0.48
38	0.3	2	-23.04	0.11
39	0	1	-22.17	
40	-0.3	2	-23.99	0.31
41	-0.75	2	-22.44	0.16

Figure S4. Range data for Permian and lower Triassic strata in Karoo Basin, compiled from ref 16 and the new data presented here. Each taxon is a genus. This graph supports our contention that significant background extinction was occurring well before the P/T event. While no equivalent graph plotted such as that presented here exists for the Hell Creek formation (with a time span of about half that shown in the Permian part of this diagram), the work of (*9*) has demonstrated that at least among dinosaurs there no decrease in taxa prior to the K/P event occurred.

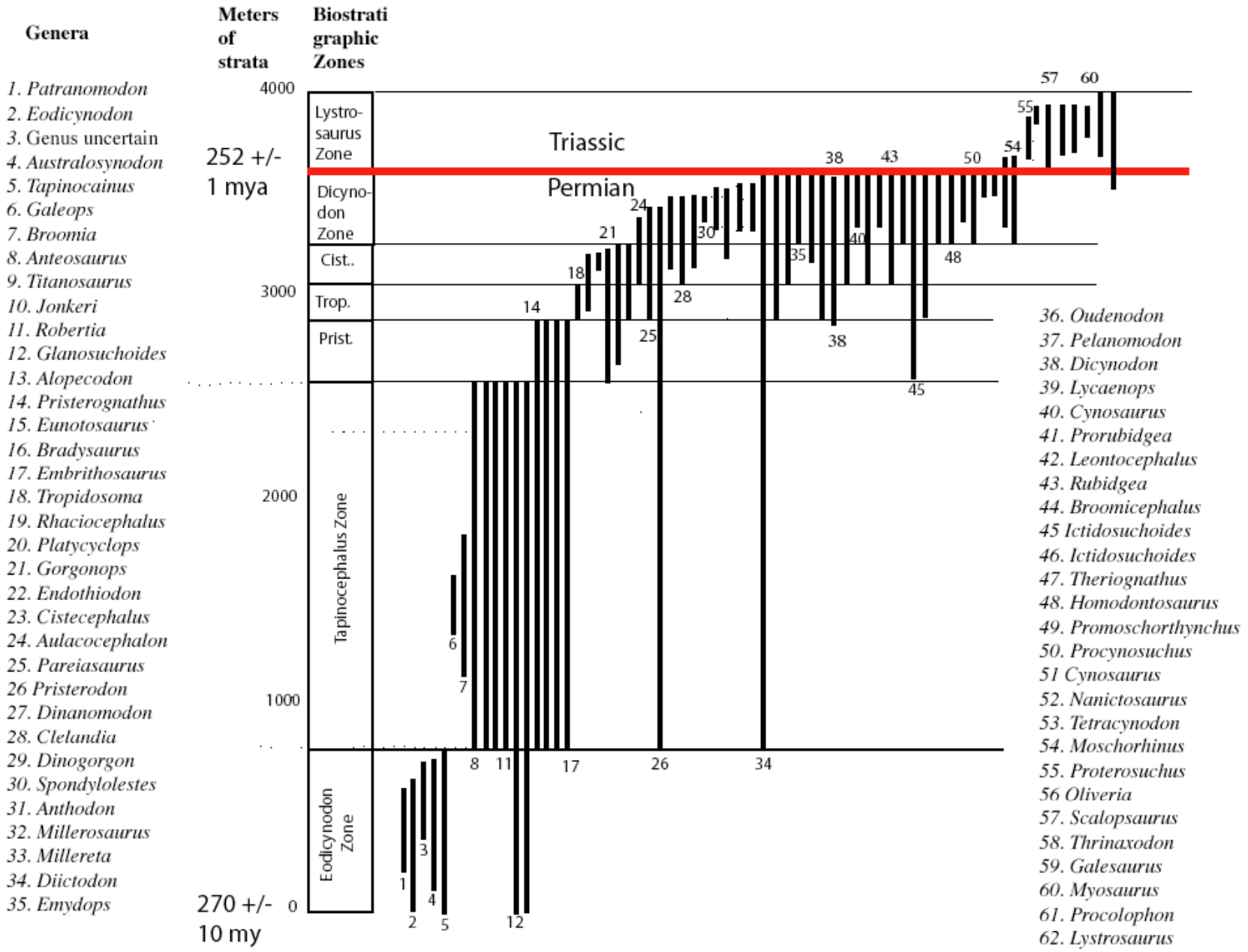
Genera
Meters of strata
Biostratigraphic Zones
1. Patranomodon
2. Eodicynodon
3. Genus uncertain
4. Australosynodon
5. Tapinocainus
6. Galeops
7. Broomia
8. Anteosaurus
9. Titanosaurus
10. Jonkeri
11. Robertia
12. Glanosuchoides
13. Alopecodon
14. Pristerognathus
15. Eunotosaurus
16. Bradysaurus
17. Embrithosaurus
18. Tropidosoma
19. Rhaciocephalus
20. Platycyclops
21. Gorgonops
22. Endothiodon
23. Cistecephalus
24. Aulacocephalon
25. Pareiasaurus
26 Pristerodon
27. Dinanomodon
28. Clelandia
29. Dinogorgon
30. Spondylolestes
31. Anthodon
32. Millerosaurus
33. Millereta
34. Diictodon
35. Emydops
4000
3000
2000
1000
0
252 +/- 1 mya
270 +/- 10 my
Lystro-saurus Zone
Dicyno-don Zone
Cist..
Trop.
Prist.
Tapinocephalus Zone
Eodicynodon Zone
Triassic
Permian
36. Oudenodon
37. Pelanomodon
38. Dicynodon
39. Lycaenops
40. Cynosaurus
41. Prorubidgea
42. Leontocephalus
43. Rubidgea
44. Broomicephalus
45 Ictidosuchoides
46. Ictidosuchoides
47. Theriognathus
48. Homodontosaurus
49. Promoschorthynchus
50. Procynosuchus
51 Cynosaurus
52. Nanictosaurus
53. Tetracynodon
54. Moschorhinus
55. Proterosuchus
56 Oliveria
57. Scalopsaurus
58. Thrinaxodon
59. Galesaurus
60. Myosaurus
61. Procolophon
62. Lystrosaurus